Noise Analysis of LSO-PSAPD PET Detector Front-End Multiplexing Circuits

Frances W. Y. Lau, Peter D. Olcott, Mark A. Horowitz, Hao Peng, and Craig S. Levin

Abstract – **We are designing a 1mm^3 resolution PET (Positron Emission Tomography) system with over twenty-thousand readout channels. Multiplexing of the PSAPD (position sensitive avalanche photodiode) detectors would simplify the readout electronics and reduce the density of the circuit board design. We used simulations and experiments to study the performance of three front-end circuit configurations, 1) no multiplexing, 2) multiplexing with single-ended preamplifiers, and 3) multiplexing with differential preamplifiers, by evaluating their energy resolution and crystal identification ability. With single-ended multiplexing, there is no degradation in energy resolution but there is some degradation in crystal identification. With the novel differential multiplexing scheme presented in this paper, in simulation, there is less than 0.1dB degradation in energy resolution and no significant degradation in crystal identification. We also present a pseudo-differential technique which can be used when differential preamplifiers are not available, which we found gives a slight improvement over single-ended multiplexing.**

I. Introduction

We are designing a 1mm^3 resolution PET (Positron Emission Tomography) system with over twenty-thousand readout channels. This system requires complex, dense interconnect between the detectors and the ASIC (application specific integrated circuit) that contains the front-end preamplifiers. Multiplexing of this analog interconnect would simplify the readout electronics and reduce the density of the circuit board design.

Multiplexing has been extensively studied for PMT (photomultiplier tube) designs [1]. However, semiconductor detectors such as PSAPDs (position sensitive avalanche photodiodes) typically have a factor of 1000 to 10,000 less gain than PMTs. This lower gain limits the number of channels that can be multiplexed together before the energy, time, and spatial resolution of the PET system are degraded. Multiplexing of digital signals has also been studied [2]. However, our constraint is the analog interconnect complexity, that is, the traces for the inputs to the ASIC, not the traces for the digital outputs of the ASIC, so digital multiplexing does not solve our problem.

Manuscript received November 23, 2007. This work was supported by NIH grants R01CA119056 and R33 EB003283 as well as the Stanford Bio-X Graduate Fellowship.

F. W. Y. Lau (email: flau@stanford.edu) is a graduate student in the Department of Electrical Engineering and P. D. Olcott is a graduate student in the Department of Bioengineering at Stanford University. M. A. Horowitz is with the Department of Electrical Engineering at Stanford. H. Peng and C. S. Levin (email: cslevin@stanford.edu) are with the Department of Radiology and the Molecular Imaging Program at Stanford.

We present three front-end circuit configurations: 1) no multiplexing, 2) single-ended multiplexing, and 3) differential multiplexing or pseudo-differential multiplexing. Using simulation and experiment, we evaluate the complexity of interconnect, energy resolution, and crystal identification of each configuration. We propose that the novel differential multiplexing scheme enables the simplification of the interconnect without significant degradation in the system performance.

II. Noise Sources

The detector consists of an LSO (Lutetium Oxyorthosilicate) scintillation crystal array coupled to a PSAPD (position sensitive avalanche photodiode). The signals are read-out using the RENA-3 ASIC from NOVA R&D. To understand the effect multiplexing will have on the system, we first need to look at sources of noise in the LSO array, the PSAPD, and the electronics.

A. LSO Scintillation Crystal Array

The LSO scintillation crystal array light output has a variance due to the spatial distribution of light produced by the crystal as well as the fact that the number of photons generated is Poisson distributed. In addition, if there is intra-array photon scatter causing interactions in PSAPDs that are multiplexed together, this may degrade the spatial resolution. However, we assume that we will choose which PSAPDs to multiplex together wisely so that this will be rare.

We chose an array with no reflectors between the crystals because crystal identification with this array will be more challenging (versus an array with intercrystal reflectors) and we wanted to evaluate the worst case scenario.

B. PSAPD

The system uses the 8x8 mm^2 PSAPD developed by Radiation Monitoring Devices (RMD), Inc. (Watertown, MA) [3]. This PSAPD has four corner contacts on the n-doped back side of the device which is covered by a high resistivity layer. The position of a flash of light is measured using these four spatial channel corner signals with Anger-type logic. The front side of the device has one contact which we call the "common". Measurements by RMD and by our group found that the bias for an optimal signal-to-noise ratio (SNR) ranged from 1730V to 1750V, resulting in a gain of approximately 1000. However, in our experiments, the ASIC was saturated if we used a bias of 1750V. We are currently working on

1-4244-0923-3/07/$25.00 ©2007 IEEE.

finding a solution to this problem so that we can operate at the ideal bias voltage. The results in this paper are for a bias of 1710V, which we assume corresponds to a gain of approximately 800 [1].

The dominant noise source in the system is the shot noise from the PSAPD due to the large leakage current which was measured to be roughly 0.9μA at a 1710V bias. There is a Poisson variance in the gain of the PSAPD as well as an excess noise factor, which we assume to be 2.5 [4], which also degrade the performance. The effect of the PSAPD flicker noise is very small at the frequencies of interest.

C. Electronics

The RENA-3 ASIC was developed by NOVA R&D (Irvine, CA) for solid state detectors [5]. It contains 36 channels of preamplifier, Gaussian shaper, trigger, sample-hold, and fast time stamp circuitry. It contains low noise charge sensitive preamplifiers, so the noise contribution of the electronics is very small. We assume it is less than 5% of the shot noise.

III. Front-end Circuit Architectures

Fig. 1a) shows the no multiplexing case. In this configuration, all four spatial channels and the common are read out separately using single-ended preamplifiers. The energy and time are measured from the common.

Fig. 1b) shows single-ended multiplexing. Here, corresponding spatial channels are connected together. This configuration is similar to that presented in [6]. The commons are kept independent (un-multiplexed) so that we can identify in which PSAPD an interaction occurred. All the signals are read out with single-ended preamplifiers. The energy and time are measured from the common terminal.

Fig. 1c) shows differential multiplexing. The corresponding spatial channels are connected together as was in the single-ended multiplexing case. The difference is that differential preamplifiers are used to amplify the signals. The commons are used as references for the differential amplifiers.

If the shot noise of the PSAPD dominates the overall noise, there is no significant degradation in the system performance with the differential multiplexing scheme. To understand this, we examine Fig. 2a), which considers the simplified situation when two diodes are multiplexed together, and there is signal and noise from the first diode but only noise from the second diode. Since current always needs a return path and current always takes the path of least impedance, only a small fraction of noise current from the second diode is coupled into the differential amplifier output of the first diode.

Fig 2b) shows why the coupling is different in the single-ended multiplexing case. Only a small fraction of the noise current from the second diode is coupled into the amplifier for the common of the first diode so there is little degradation in the common signal. However, noise is coupled into the spatial channels, unlike the differential multiplexing case.

From this analysis of the single-ended multiplexing case, an interesting observation can be made: the noise from the second diode entering the common of the first diode and its spatial channels are correlated. Therefore, if we knew what fraction of current goes into which branch, we can do post-processing by scaling the outputs and then subtracting to eliminate that noise contribution. We call this technique "pseudo-differential". This technique is not as robust as the true differential scheme because it is difficult to accurately estimate the fraction of current that goes into each branch for the subtraction. Also, a true differential architecture has the added benefit of being more robust to external electrical interference. However, when no differential amplifiers are available, the pseudo-differential method is a good technique to consider.

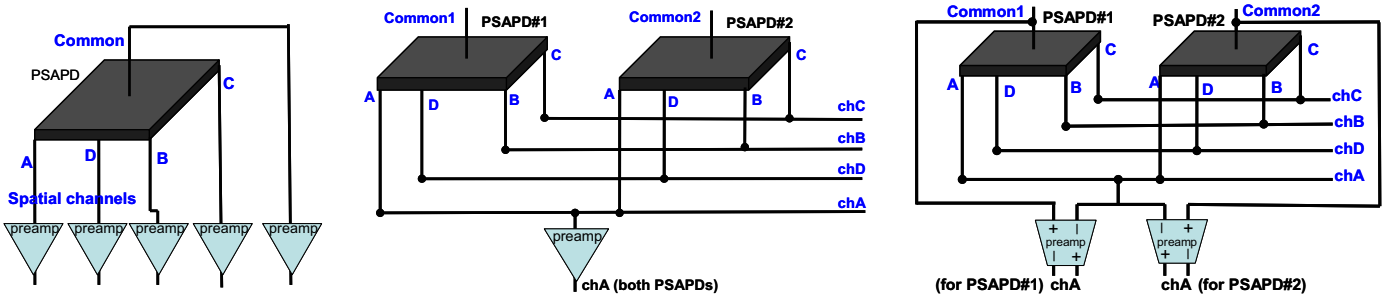

a) No multiplexing b) Single-ended multiplexing c) Differential Multiplexing

Fig. 1. Front-end circuit architectures. In B) and C), only the preamplifiers for channel A are shown for simplicity. Note that each preamplifier consists of an op-amp with a feedback network consisting of a capacitor in parallel with a resistor (not shown). There are also AC coupling capacitors and bias resistors between the PSAPD outputs and the preamplifier inputs (not shown).

[1] This is not the ideal operating point so the performance metrics extracted are not as good as we hope they will be in the future. However, for comparison purposes, this operating point should be sufficient because we use the same parameters for all three cases compared.

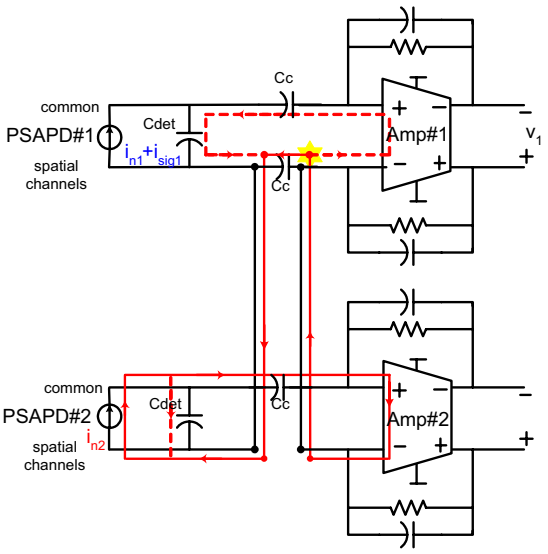

a) Schematic diagram for differential multiplexing, including noise coupling paths (in red)

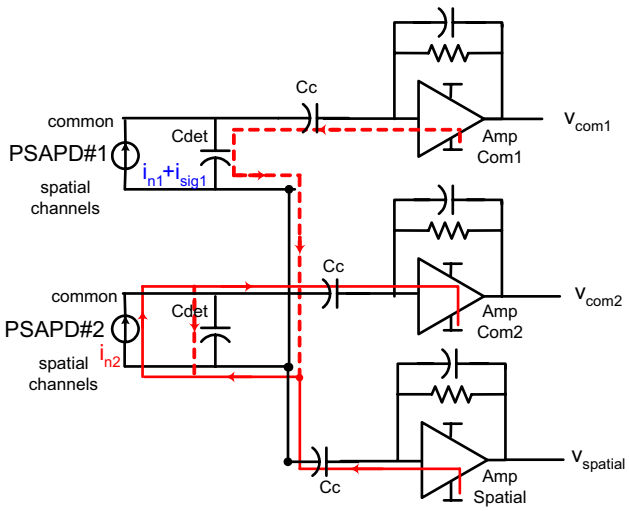

b) Schematic diagram for single-ended multiplexing, including noise coupling paths (in red)

Fig. 2. Drawing of the flow of the current from the PSAPD to understand how noise couples into the output. To simplify the diagram, we substitute the PSAPD with a two terminal diode. C_{det} is the detector capacitance and C_c is the AC coupling capacitor. We assume PSAPD #1 has signal i_{sig1} and noise i_{n1} but PSAPD #2 only has noise i_{n2}. The red lines indicate the path of the flow of noise current i_{n2}. Current flows in loops so the current flowing out of the PSAPD needs a return path. A larger fraction of current will take the path of least impedance as the return path. The dotted red line indicates that a smaller fraction of current would take that path because that path has higher impedance than the path with the solid red line.

In a), at the junction point marked with the yellow star, the path directly back to PSAPD#2 is much lower impedance than the path that goes into Amp#1 (the path through Amp#1 goes through the PSAPD#1 detector capacitance). Therefore, there is very little noise current from PSAPD#2 coupling into Amp#1. Note that the differential input impedance of the preamplifiers is low, so most of the current goes in one input and out the other input.

In b), after the current goes into AmpCom2, it needs to return to PSAPD#2. Therefore, it goes into the ground (or supply), which is connected to the ground (or supply) of the other preamplifiers, so the current returns to PSAPD#2 through the other preamplifiers. Only a small fraction will return through AmpCom1 because that path has much larger impedance.

IV. Methods

A. Simulation Circuit Model

We modeled the PSAPDs, bias circuitry, and preamplifiers as lumped circuit elements using H-SPICE and Verilog-A. The PSAPD was represented as a capacitor in parallel with a current source. Fig 3 illustrates the circuit model for the PSAPD.

The outputs of this PSAPD circuit model are connected to preamplifiers using the architectures in Fig. 1. To evaluate the noise performance, we graphed the power spectral density of the total noise at the output of the preamplifier for a particular channel. Then, we multiplied the power spectral density by the square of the band-limiting shaper transfer function H(s), integrated over frequency, and computed the square root of the result to obtain the RMS (root-mean-square) integrated output referred noise (V_{rms}).

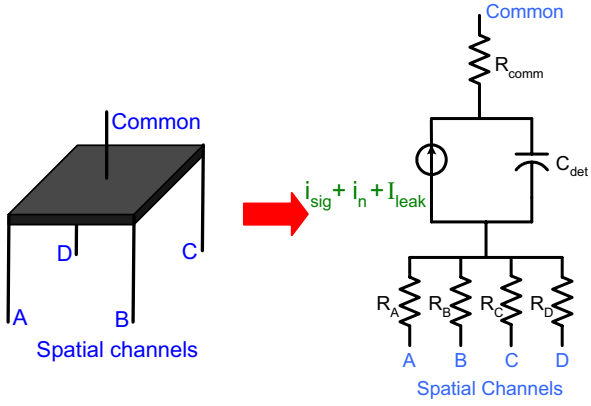

Fig. 3. Circuit model for PSAPD. C_{det} is the detector capacitance. i_{sig} is the photodetection signal. i_n is the noise (shot noise and flicker noise). I_{leak} is the sum of the DC bulk and surface leakage currents. R_{comm} is the resistance of the contact for the common terminal. R_A, R_B, R_C, and R_D are the resistances from the point of interaction to the respective corner contact, which change depending on the location of the interaction.

B. Simulation of Crystal Identification

To gauge the potential difference in spatial resolution for the architectures, we compared their crystal identification results.

With simulation we considered two cases: 1) interactions at the center and 2) interactions that are not at the center of the

PSAPD. For interactions at the center, the light distribution has no effect on crystal identification because we assume that the current produced will divide evenly to the four corners of the PSAPD. Therefore, we only need to look at the SNR of one spatial channel.

The shot noise due to the signal current is ignored because it cancels out in the calculation of the position of the interaction. If we assume that the shot noise due to leakage current is much smaller than the signal plus the shot noise due to the signal current (we found it was less than 1.6%), then the shot noise due to the signal increases the signal by a constant multiplicative factor (because the shot noise due to the signal is proportional to the signal). Since the position of the interaction is calculated from the ratio of the signals measured on the spatial channels (see equations (1) and (2)), the effect of the shot noise due to the signal current cancels out.

When the interaction is not at the center, the light distribution affects the crystal identification. Fig. 4 illustrates the simulation flow. For each crystal in the array, we choose a Poisson distributed number N which represents the number of light photons created by a 511keV photon interacting in that crystal. We use Detect2000 to simulate the spatial distribution of the light photons produced by that crystal. For each light photon, we use the Finite Element Model from [7] to calculate the resistance to the four corners. Then, we calculate the signal at each corner due to all the light photons.

We also consider the effect of the leakage current contribution to the shot noise. The H-SPICE simulation gives the Gaussian distribution of the signals at the corners due to this shot noise and we randomly sample from this distribution to get one noise value for each corner.

We combine the signal at each corner with the noise value for each corner to get the net signal for each corner. Then, we use the following formulas to calculate the position (x, y) of the interaction:

$$x = \frac{(A-B)+(D-C)}{A+B+C+D} \quad (1)$$

$$y = \frac{(A-D)+(B-C)}{A+B+C+D} \quad (2)$$

We repeat this entire process for 1000 values of N representing 1000 511 keV photon interactions in that crystal and get a 2-D histogram function for the (x, y) locations for that crystal. Then, we repeat this for every crystal in the array to obtain a 2-D histogram (flood) for the entire array. We segment the crystals in the flood image and fit a Gaussian to the histogram for each crystal. The distance between the peaks and the standard deviation of the peaks are two parameters that measure the crystal identification ability of a given configuration.

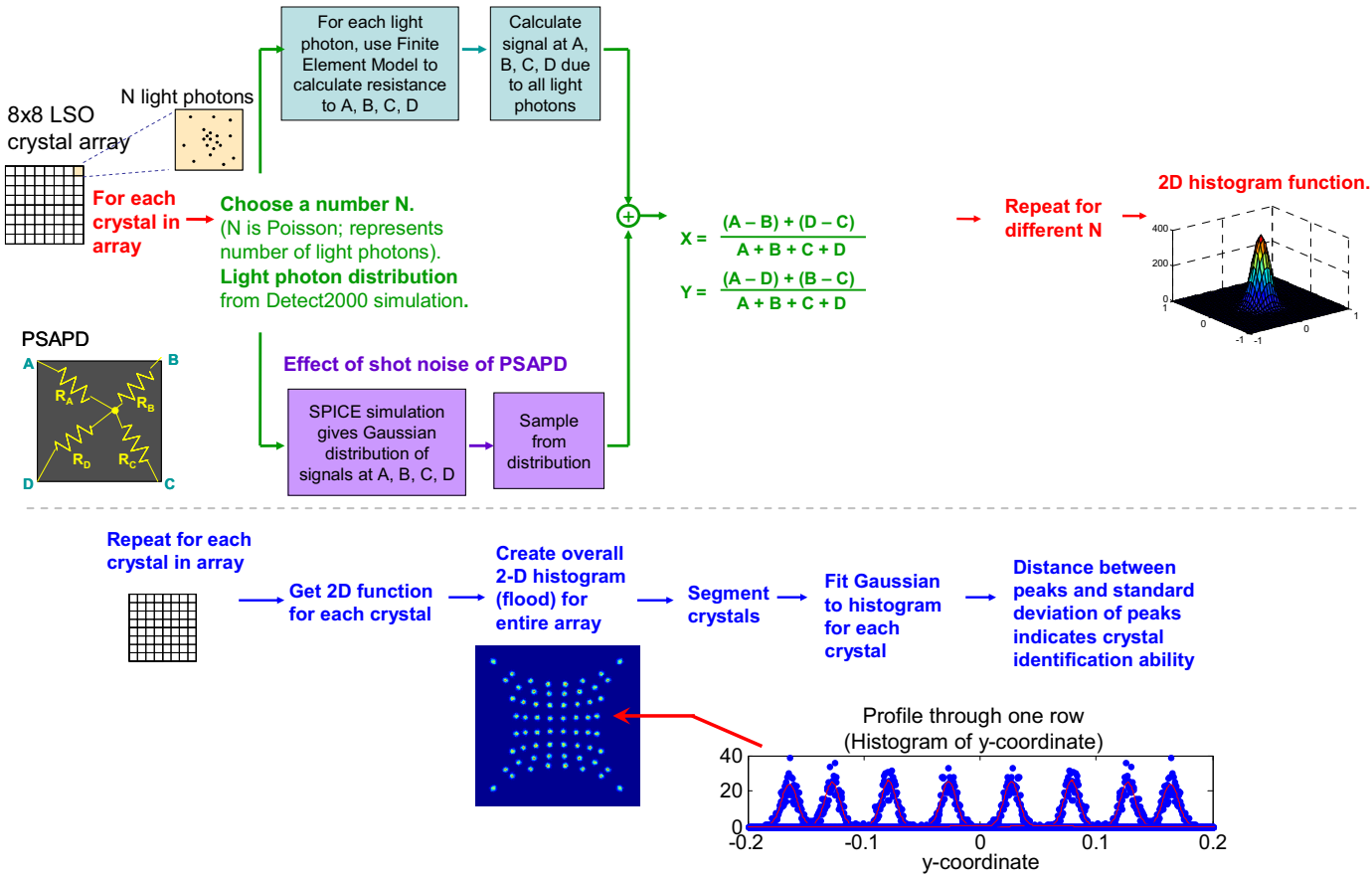

Fig. 4. Simulation flow for creating a simulated "flood histogram", used to evaluate the crystal identification ability for the case where the interaction is not at the center of the PSAPD.

C. Experimental Setup

We coupled the 1cm^2 PSAPD to an 8x8 array of 1mm^3 LSO scintillation crystals. We irradiated the detector with a 4μCi Na-22 source. To evaluate the energy resolution for the different configurations, we compared the full-width-half-max (FWHM) of the 511keV peak of the energy spectrum of the common.

We were not able to experimentally verify our differential multiplexing configuration because we did not have an ASIC with true differential amplifiers readily available. The development of discrete or integrated circuits with differential preamplifiers is for our future work. However, were able to test the pseudo-differential technique described in Section III. Therefore, for this conference paper, the experimental "differential" results we present will be for the pseudo-differential multiplexing technique.

V. Results

The performance of the architectures was compared using four performance metrics: A) complexity of interconnect, B) energy resolution, C) time resolution, and D) crystal identification.

A. Complexity of Interconnect

Fig. 5 shows how the number of wires and the number of preamplifiers scales with the number of PSAPDs multiplexed together. The required interconnect for single-ended multiplexing is the same as for the case of differential multiplexing. The number of preamplifiers required for the differential multiplexing case is actually the same as the no multiplexing case. However, this is not a concern in our system because today we can fit so many transistors on a chip that the main constraint is the interconnect, not the number of preamplifiers.

B. Energy Resolution

From simulation and experiment, we found that there was insignificant energy resolution degradation for all three architectures. This was expected since the common terminal, where the energy (and time) signal are extracted, is not multiplexed.

The energy resolution was evaluated in simulation by comparing the SNR of the common terminal, or the sum of the spatial channels for the differential multiplexing case. Table I shows that there is less than 0.1dB variation in SNR in all three cases.

TABLE I
SNR OF COMMON TERMINAL (TO CHARACTERIZE ENERGY RESOLUTION)

	# of PSAPDs	Channel	SNR (dB)
1. No multiplexing	1	Common	21.2
2. Single-ended	2	Common	21.2
	3	Common	21.2
	4	Common	21.2
3. Differential	2	Sum of spatial channels	21.1
	3	Sum of spatial channels	21.1
	4	Sum of spatial channels	21.1

Experimentally, from the energy spectrum of the common shown in Fig. 6, we see that there is no significant degradation in 511 keV photopeak energy resolution. There is a slight 0.6% degradation with the pseudo-differential scheme, but this is likely because it is not true differential multiplexing.

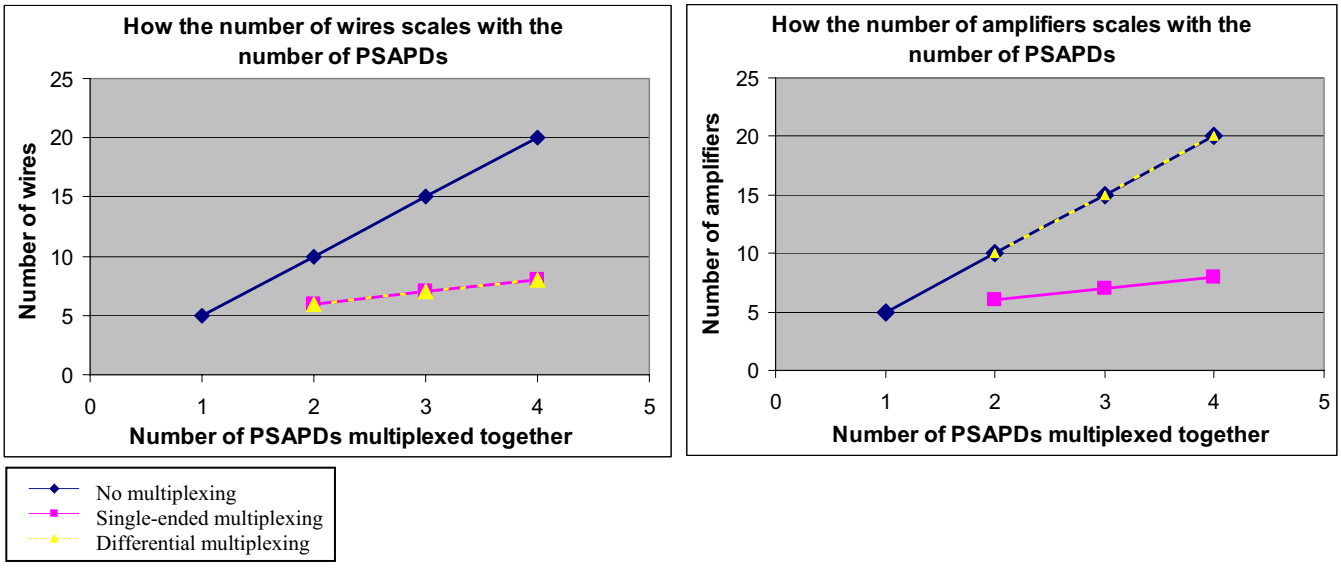

Fig. 5. How the number of wires (i.e., the interconnect) and the number of amplifiers scale with the number of PSAPDs multiplexed together.

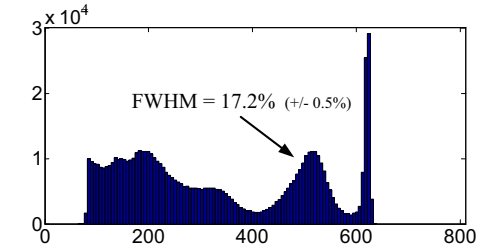

a) No multiplexing

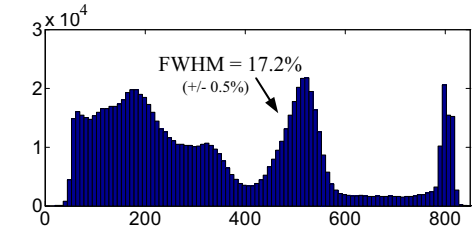

b) Single-ended multiplexing (of two PSAPDs)

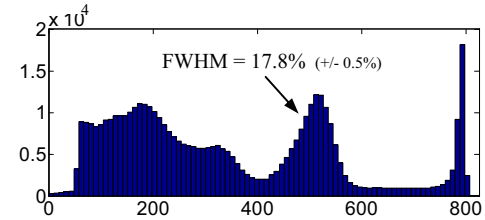

c) Pseudo-differential multiplexing (of two PSAPDs)

Fig. 6. Energy spectrum of signal from common terminal, used to determine FWHM of the 511keV peak, which indicates the energy resolution. Note that this is the global energy spectrum (i.e., summed over all crystals). The energy resolution improves substantially when we measure the per-crystal energy resolution. The same user-adjustable amplifier settings (e.g., gain) were used for all three cases. The reason the clipping threshold is lower for a) is because the capacitance seen at the input of the amplifier changes if we multiplex.

C. Time resolution

The time resolution has not been explicitly measured yet; that is for future work. However, there should not be any degradation in time resolution with multiplexing since the timing information is extracted from the common signal, which is un-multiplexed in our proposed configurations. That is because if we do a rough estimate, the time resolution assuming a perfect timing discriminator that has no time walk effects is [8]:

$$time\ resolution\ \ (FWHM) = \frac{V_{no}}{(dV_o / dt)} \qquad (3)$$

V_{no} is the RMS noise voltage at the output of the preamplifier, and we showed in the energy resolution section that this does not change significantly for all three architectures. dV_o/dt is the slope of the voltage at the output of the preamplifier, and since the common terminal is not multiplexed, there is very little change in this slope.

D. Crystal Identification

To evaluate the crystal identification ability for interactions at the center, we evaluated the SNR of one spatial channel. Table II shows that there is degradation for single-ended multiplexing but no degradation for differential multiplexing. The SNR for the spatial channels is higher than the SNR for the common terminal because the shot noise due to the signal current cancelled as explained in Section IV.B.

We observed a small increase in SNR for the differential architectures compared to the no multiplexing case. Part of this change is due to the intrinsic SNR benefit of differential architectures. The output of differential circuits has twice the signal but only $\sqrt{2}$ of the uncorrelated noise. To examine whether we see this effect in our circuit, we considered the additional case where we have no multiplexing but use differential amplifiers, and found that the SNR is 41.7dB, slightly larger than the no multiplexing case with single-ended amplifiers (41.6dB). We only see a 0.1dB improvement in SNR because our system is dominated by correlated PSAPD noise, not uncorrelated noise. The slight differences in SNR observed for the differential architectures (i.e., differential architecture with 1, 2, 3, or 4 PSAPDs) is currently under investigation. They may be caused by simulation artifacts or second order effects that are presently not modeled or fully understood.

TABLE II
SNR OF SPATIAL CHANNELS

	# of PSAPDs	Channel	SNR (dB)
1. No multiplexing	1	Ch A	41.6
2. Single-ended multiplexing	2	Ch A	39.4
	3	Ch A	38.1
	4	Ch A	37.1
3. Differential multiplexing	2	Ch A	43.1
	3	Ch A	43.5
	4	Ch A	43.8

The simulation results for interactions in crystals that are not at the center of the PSAPD are presented in Fig. 7. There is degradation in crystal identification with single-ended multiplexing, but no significant degradation with differential multiplexing.

Fig. 8 shows the flood histograms obtained experimentally. There is degradation in spatial resolution with the single-ended multiplexing scheme, especially at the corners. Although not as good as if we had true differential preamplifiers, we see an improvement with the pseudo-differential technique.

To quantify the results, we compare a figure of merit (FoM) which we define as:

$$\text{FoM} = \frac{distance\ between\ peaks}{standard\ deviation\ of\ \ peak} \qquad (4)$$

A larger FoM indicates superior crystal identification. The FoM was computed for each crystal. The average for the edge crystals and the average for the middle crystals were computed separately and the results are in Table III.

TABLE III
COMPARISON OF FIGURE OF MERIT
OF DIFFERENT MULTIPLEXING SCHEMES VIA EQUATION (4)

	Simulation		**Experiment**	
	Edge crystals	**Middle crystals**	**Edge crystals**	**Middle crystals**
1. No multiplexing	12.018 ± 0.003	19.507 ± 0.002	3.75 ± 0.01	6.146 ± 0.008
2. Single-ended multiplexing (of 2 PSAPDs)	9.555 ± 0.003	14.994 ± 0.002	3.5 ± 0.1	5.5 ± 0.1
3. Differential multiplexing (of 2 PSAPDs)	13.614 ± 0.003	22.316 ± 0.002	**Pseudo-differential** 3.7 ± 0.2	**Pseudo-differential** 5.71 ± 0.02

VI. DISCUSSION

With differential multiplexing, we can reduce the amount of interconnect required without significantly degrading the energy resolution and crystal identification ability.

Comparing Fig. 7 and Fig. 8 and examining Table III, the crystal identification ability is better with the simulated flood than the experimental flood. There are some secondary effects that are not modeled in simulation which we are currently investigating. For example, scattered and random interactions are not modeled in simulation. Also, in experiment, crystals at the edge of the array receive fewer counts.

An interesting question that is currently under investigation is: what limits the extent of multiplexing that can be implemented? First of all, the availability of differential amplifiers is an important factor. We currently do not have differential amplifiers readily available in an ASIC, so the number of PSAPDs we can multiplex together is limited. In addition, if a large number of PSAPDs are multiplexed together, it would be difficult to select PSAPDs to multiplex together that are in close proximity to each other without considerably increasing the probability of two or more interactions occurring in multiplexed PSAPDs due to inter-array scatter, which could degrade the spatial resolution and contrast. Finally, the preamplifier noise, PSAPD noise, detector capacitance, and AC coupling capacitance affect the degree of multiplexing possible.

VII. CONCLUSION

We can reduce the complexity of the analog interconnect in our PET system using multiplexing of PSAPD signals. With single-ended multiplexing, there is no degradation in energy resolution but there is some degradation in crystal identification. With the novel differential multiplexing scheme presented in this paper, there is no significant degradation in energy resolution and crystal identification. When differential amplifiers are not available, the pseudo-differential technique presented gives a slight improvement over the single-ended multiplexing technique.

ACKNOWLEDGMENT

We thank Paul Reynolds for assisting with the data acquisition for the experimental results as well as all the members of the Molecular Imaging Instrumentation Lab for their input and suggestions. We thank Richard Farrell of RMD Inc. (Watertown, MA) for his advice on the PSAPD modeling.

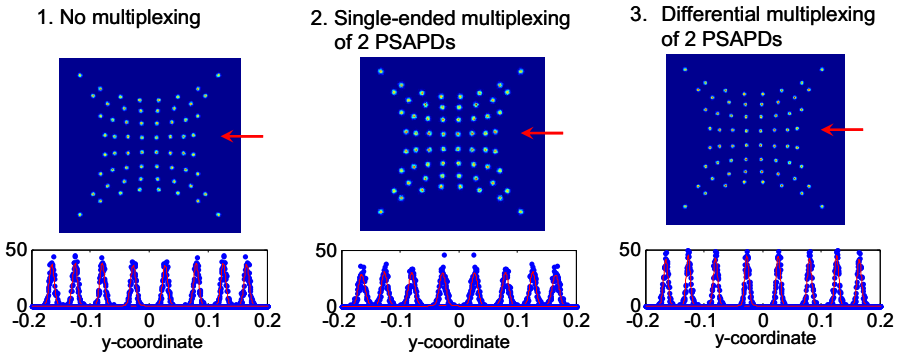

Fig. 7. Simulation results – flood histograms and example of the profile through one row of the flood

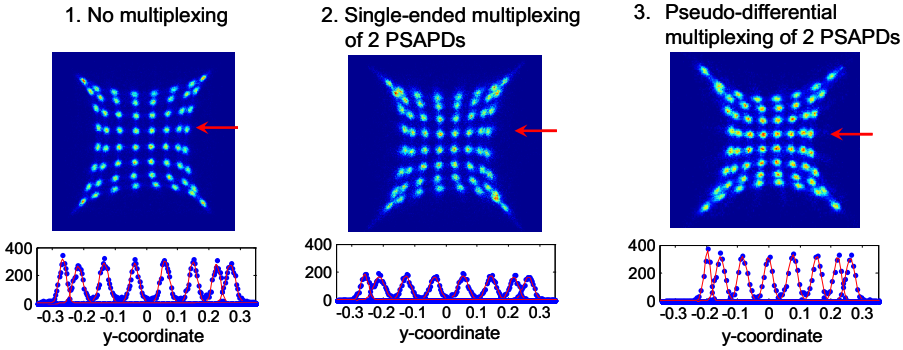

Fig. 8. Experimental results – flood histograms and example of the profile through one row of the flood

REFERENCES

[1] P. D. Olcott, J. A. Talcott, C. S. Levin, F. Habte, A. M. K. Foudray, "Compact Readout Electronics for Position Sensitive Photomultiplier Tubes," *IEEE Trans. Nucl. Sci.,* vol 52, no. 1, pp 21-27, Feb. 2005.

[2] K. Shimazoe, J. Yeom, H. Takahashi, T. Kojo, Y. Minamikawa, K. Fujita, H. Murayama, "Multi-Channel Waveform Sampling ASIC for Animal PET System," in *IEEE Nuclear Science Symposium Conference Record,* 2006, vol.4, pp. 2473-2475.

[3] K. S. Shah, R. Farrell, R. Grazioso, E. S. Harmon, and E. Karplus, "Position-sensitive avalanche photodiodes for gamma-ray imaging," *IEEE Trans Nucl Sci*, vol. 49, no. 4, pp. 1687-1692, Aug 2002.

[4] K. S. Shah, "A Novel Position Sensitive Detector for Nuclear Radiation," Report submitted to the Department of Energy, RMD Inc., Watertown, MA, 2005.

[5] T. O. Tümer, V. B. Cajipe, M. Clajus, F. Duttweiler, S. Hayakawa, J. L. Matteson, A. Shirley, O. Yossifor. "Test results of a CdZnTe pixel detector read out by RENA-2 IC," Presented at the *14th International Workshop on Room-Temperature Semiconductor X-Ray and Gamma-Ray Detectors*, 2004, and submitted to *IEEE Trans. Nucl. Sci.*

[6] P. D. Olcott, F. Habte, J. Zhang, C. S. Levin, "Charge multiplexing readout for position sensitive avalanche photodiodes," in *IEEE Nuclear Science Symposium Conference Record*, 2005, vol.5, pp. 2935-2937.

[7] P. D. Olcott, J. Zhang, C. S. Levin, F. Habte, A. M. K. Foudray, "Finite element model based spatial linearity correction for scintillation detectors that use position sensitive avalanche photodiodes," in *IEEE Nuclear Science Symposium Conference Record,* 2005, vol.5, pp. 2459-2462.

[8] H. Spieler, "Fast Timing Methods for Semiconductor Detectors," *IEEE Trans Nucl Sci*, vol.29, no.3, pp.1142-1158, June 1982.